Shock and Vibration 13 (2006) 505–518
IOS Press

Reduction of contact forces in a rotor-stator-system in case of rubbing through active auxiliary bearing

Alvaro Chavez*, Heinz Ulbrich and Lucas Ginzinger
Institute of Applied Mechanics, Technical University of Munich, Germany

Abstract. The present manuscript deals with the problem of rotor-stator rubbing. Due to performance increase in rotating machinery, rubbing processes happen more frequently. These are very complicated mechanisms that lead to high impact loads, vibrations and instability. The authors propose a control technique by using an active auxiliary bearing to overcome the problem of rubbing. The control concept enables a transition of the rotor towards a contact situation (with an auxiliary bearing) without rebounding and loss of contact. To investigate the practical feasibility of this approach, numerical simulation has been used to show that using this control concept the impulse (and contact force respectively) can be significantly decreased. Experiments to validate the theoretical findings are already in progress and will be published soon.

Keywords: Active auxiliary bearing, rotor-to-stator rubs, unilateral contact, time stepping

1. Introduction

Because of the continuous performance increase of turbo machines it comes to rubbing between components of the rotor and the housing. These unwanted rubbing processes are complicated mechanisms which induce vibrations with the consequence of emerging contact forces, causing not only high impact loads, but also a multitude of vibrations with large amplitudes or even instabilities. This can lead to heavy damage of the machine or to complete destruction. In order to avoid this, a method has been investigated with the help of controlled active bearings to minimize the contact forces. An auxiliary bearing exerts control forces on the rotating system, which is connected to the base through electromagnetic actuators. Because of problem specific control strategies multi impacts during rubbing can be avoided and the amplitude of the single impacts can be drastically reduced, which will be shown by numeric simulations.

Several authors presented control concepts for minimizing the contact forces in rotor systems. For example, Jiang and Ulbrich [7] developed optimal control for a Laval rotor. This control design bases on a stability investigation, when the system is in full annular rub. This means that the amplitude and the frequency of the vibrations of the rotor and the auxiliary bearing are both the same and constant. Ulbrich et al. [16] showed that it is possible to reduce the contact force between the flexible rotor and the auxiliary bearing. The controller has been activated before the first contact occurs. Therefore a smooth transition to full annular rub is ensured. Yigit and Christouforou [17] used a linearized drill model and a quadratic cost functional to cancel vibration from friction between bore hole and drill. On the other hand, numerous interesting research publications about impact loads in robotic systems have been published in the last decade, Brogliato [4], Tornambè [14], but the problem of controlling the impact is still open.

*Corresponding author: Alvaro Chavez, Institute of Applied Mechanics, Technical University of Munich, Germany. Tel.: +49 89 289 15199; Fax: +49 89 289 15213; E-mail: chavez@amm.mw.tum.de.

ISSN 1070-9622/06/$17.00

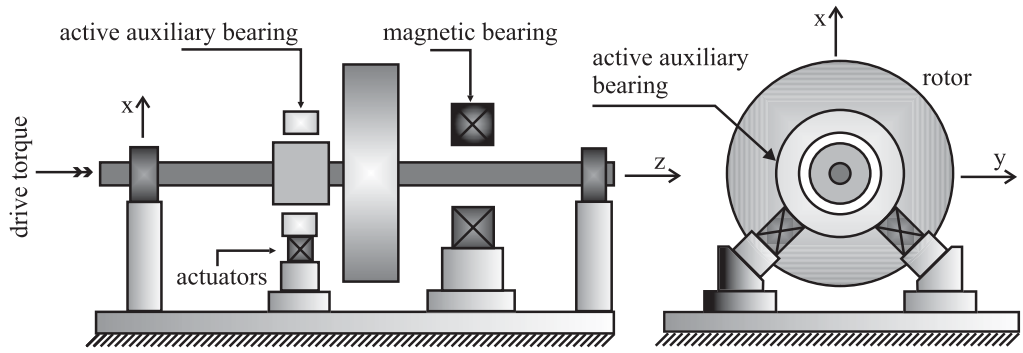

Fig. 1. Active rotor-auxiliary bearing system.

The difficulty is related to a sudden change of the equations of motion when there is a switch from a state of no contact to contact condition.

The outline of this paper is as follows. Section 2 outlines the equations of motion of the system, the flexible rotor and the active auxiliary bearing. The use of a rigid contact model is used in Section 3, to model the impact between rotor and auxiliary bearing. Subsequently Section 4 deals with the control scheme formulation. The transition phase from the free motion state to the constrained state without rebounds will be shown in Section 5 through the simulation of the dynamics. The test rig is described in Section 6 and finally the conclusions of this work are drawn in Section 7.

2. Modeling of the equations of motion

The computer model of the mechanical system is modeled by a hybrid multibody system (HMBS) method. The HMBS approach is useful when active components are included, Ulbrich [15]. This method assures a modular and physical transparent description of complex dynamical systems, Bremer [2,3].

The active rotor-auxiliary bearing system consists of an elastic rotor, which is pivoted over two isotropic ball bearings, an auxiliary bearing connected to two electromagnetic actuators with 45 ° alignment attached to the base, a magnetic bearing to create realistic stimulation and an asynchronous motor as a controlled driving unit with a characteristic torque-speed curve.

2.1. Rotor

The mechanical modeling characterized the rotor as an elastic shaft, which is held by two passive bearings with linear characteristic curves. The rotor has a continuous mass distribution and has been modeled by the Euler-Bernoulli beam theory. The elastic deformation of the beam takes into account the bending and the torsion which are considered small and of first order. Inertia, material damping, gyroscopic effects, elastic forces, rotations symmetry and spin are also take into account in the mathematical model.

The elastic deformation of the rotor as a function of time t and the location of the beam element expressed by a coordinate z along the rotor axis can be represented by the Ritz approximation functions

$$\begin{aligned} u(z,t) &= \mathbf{u}^T(z)\mathbf{q}_{r_u}(t)\,; \quad v(z,t) = \mathbf{u}^T(z)\mathbf{q}_{r_v}(t)\,; \quad \mathbf{u},\, \mathbf{q}_{r_u},\, \mathbf{q}_{r_v} \in \mathsf{R}^{n_b}\,; \\ \vartheta(z,t) &= \vartheta^T(z)\mathbf{q}_{r_\vartheta}(t)\,; \quad \vartheta,\, \mathbf{q}_{r_\vartheta} \in \mathsf{R}^{n_t}\,; \end{aligned} \tag{1}$$

where the elements of these vectors $\mathbf{u}$ and ϑ are admissible shape functions, with n_b and n_t as the number of shape functions in bending and torsion respectively. The relevant eigenfunctions of the rotor at the nominal frequency are displayed in Fig. 2.

The derivation of the equations of motion of the rotor has been done by using the theorems of linear and angular momentum. Description of the rotor system took place in the fixed Cartesian coordinates so that the center line of

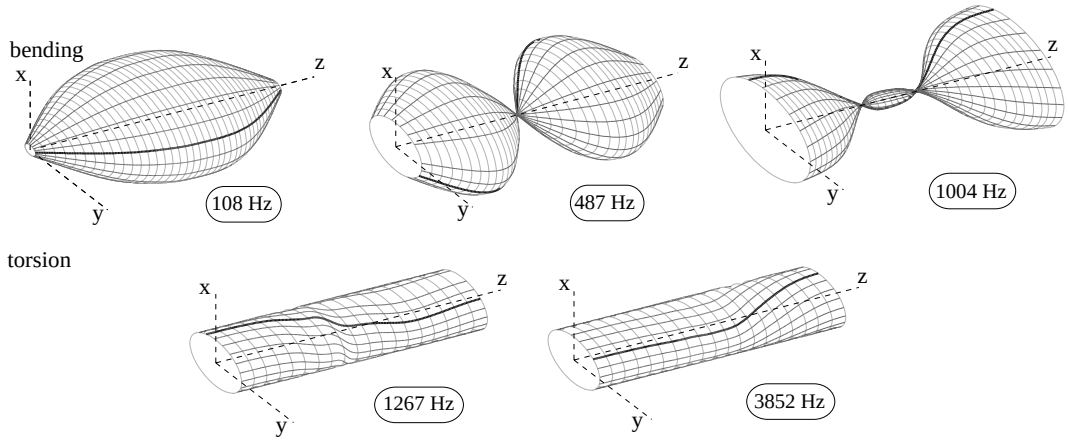

Fig. 2. Eigenmodes of the rotor $\Omega_{nom} = 50$ Hz.

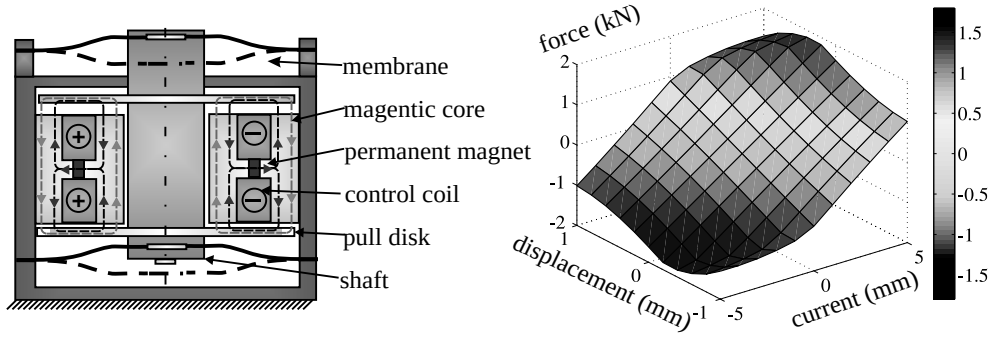

Fig. 3. Schematic of the actuator (left), force-field of the actuator (right).

the shaft lies on the z-axis. From this follows

$$\mathbf{M}_r\ddot{\mathbf{q}}_r + [\mathbf{D}_r + \mathbf{G}_r(\Omega)]\dot{\mathbf{q}}_r + [\mathbf{S}_r + \mathbf{N}_r(\dot{\Omega},\ \Omega)]\mathbf{q}_r = \mathbf{h}_r\ . \tag{2}$$

$\mathbf{M}_r$ is the mass matrix, $\mathbf{D}_r + \mathbf{G}_r$ is the damping and skew gyroscopic matrix , $\mathbf{S}_r + \mathbf{N}_r$ is the stiffness and the skew circulatory symmetric matrix. Vector $\mathbf{h}_r$ is the generalized external force. Vector $\mathbf{q}_r(t) = [\mathbf{q}_{r_u}^T(t)\ \mathbf{q}_{r_v}^T(t)\ \mathbf{q}_{r_\vartheta}^T(t)]^T \in \mathrm{R}^{n_r}$ is representing the generalized coordinates. The calculation of the matrices is pointed out in detail by Bremer and Pfeiffer [3], Bremer [2], Ulbrich [15], and others.

2.2. Active auxiliary bearing

The schematic of the active auxiliary bearing is shown in Fig. 1. The active support of the auxiliary bearing is realized by two electromagnetic actuators in a 45° mounting, whereby the stiffness is rotational symmetric.

An electromagnetic actuator capable of applying forces to the rotor indirectly via the auxiliary bearing is shown in Fig. 3 (left). The scheme shows a cross section of this active element, consisting mainly of two pull disks fixed on the shaft. Two annular membranes realize a frictionless support of the movable shaft with a very high radial stiffness and radial flexibility. To generate the actuator force, a high energy pre-magnetization circuit (bias-flux by highly energized permanent magnets) is superimposed by a magnetic control field, excited by the control coils operated in differential mode. The mathematical description of the unidirectional electromagnetic actuator is completely described in Oberbeck [9].

The actuator is able to generate forces up to 1 kN and has a maximum stroke of 1 mm. The Fig. 3 (right) shows the characteristic curve (static force-field), obtained by the variation of the control current and the displacement.

The mechanical model of the active auxiliary bearing is assumed as a rigid body, which is connected through damper-spring elements at the housing of the actuator to the base. The equation of motion of the active element is

$$\mathbf{M}_a\ddot{\mathbf{q}}_a(t) + \mathbf{D}_a\dot{\mathbf{q}}_a(t) = \mathbf{u}_a(\mathbf{q}_a, \mathbf{i}) \,, \tag{3}$$

where $\mathbf{q}_a \in \mathrm{R}^2$ as the degree of freedom in x, and y direction. $\mathbf{M}_a$ is the mass matrix of the auxiliary bearing and the actuator. $\mathbf{D}_a$ is the matrix for the outer damping. $\mathbf{u}_a(\mathbf{q}_a, \mathbf{i})$ is the force vector of the characteristic curve for both actuators.

3. Contact kinematics

The contact law is formulated by the non-smooth characteristic curve as described in Pfeiffer and Glocker [10] (1996), Glocker [6] (1995). Following the arguments of these authors, a unilateral contact can be opened or closed during the time dependent process. When the contact is closed (active contact) a pressure force can be transferred through the contact point.

In order to analyze the contact kinematics, a generalized n-dimensional vector $\mathbf{q}$ is defined. The vectors $\mathbf{q}_r$ and $\mathbf{q}_a$, which are defined by Eqs (2) and (3), respectively have dimensions equal to n_r and 2, where

$$\mathbf{q} = [\mathbf{q}_r^T \; \mathbf{q}_a^T]^T \quad \in \mathrm{R}^n. \tag{4}$$

The matrices $\mathbf{J}_{T,a},\ \mathbf{J}_{T,r},\ \mathbf{J}_{R,r}$ are defined as

$$\mathbf{J}_{T,a} = \begin{bmatrix} \mathbf{0}\,\mathbf{0}\,\mathbf{0}\,1\,0 \\ \mathbf{0}\,\mathbf{0}\,\mathbf{0}\,0\,1 \\ \mathbf{0}\,\mathbf{0}\,\mathbf{0}\,0\,0 \end{bmatrix},$$

$$\mathbf{J}_{T,r} = \begin{bmatrix} \mathbf{u}^T(z) & \mathbf{0} & \mathbf{0}\,0\,0 \\ \mathbf{0} & \mathbf{u}^T(z) & \mathbf{0}\,0\,0 \\ \mathbf{0} & \mathbf{0} & \mathbf{0}\,0\,0 \end{bmatrix} \quad \in \mathrm{R}^{3\times n}, \tag{5}$$

$$\mathbf{J}_{R,r} = \begin{bmatrix} \mathbf{0} & -\mathbf{u}'^T(z) & \mathbf{0} & 0\,0 \\ \mathbf{u}'^T(z) & \mathbf{0} & \mathbf{0} & 0\,0 \\ \mathbf{0} & \mathbf{0} & \vartheta^T(z) & 0\,0 \end{bmatrix}.$$

In Eq. (5), $\mathbf{J}_{T,r}$ and $\mathbf{J}_{R,r}$ are the translatory and the rotatory Jacobian Matrices and $\mathbf{J}_{T,a}$ is the translatory Jacobian Matrix of the active auxiliary bearing. $\mathbf{u}(z)$, $\vartheta(z)$ are the vectors of the shape functions of the rotor and $\mathbf{u}'(z)$ the derivative of $\mathbf{u}(z)$.

Figure 4 shows the cross section of the auxiliary bearing and the rotor before contact. Thereby is $\delta = |\overrightarrow{P_1P_2}|$, $\mathbf{n}_1$, $\mathbf{t}_1$ normal and tangential vector and $\widetilde{\mathbf{e}_3}$ the basis vector of the z-axis with

$$\begin{aligned} \delta &= \sqrt{\mathbf{q}^T[\mathbf{J}_{T,r} - \mathbf{J}_{T,a}]^T[\mathbf{J}_{T,r} - \mathbf{J}_{T,a}]\mathbf{q}} \,, \\ \mathbf{n}_1 &= -\delta^{-1}[\mathbf{J}_{T,r} - \mathbf{J}_{T,a}]\mathbf{q} \,, \\ \mathbf{t}_1 &= \widetilde{\mathbf{e}_3}\mathbf{n}_1 \,. \end{aligned} \tag{6}$$

The distance between the contact points (s_1, s_2) in Fig. 4 can be formulated in the following way:

$$\begin{aligned} g_N &= -\mathbf{r}_D^T\mathbf{n}_1 \qquad\qquad = \delta_0 - \delta \,, \\ \dot{g}_N &= \mathbf{v}_{s1}^T\mathbf{n}_1 + \mathbf{v}_{s2}^T\mathbf{n}_2 = \delta^{-1}\mathbf{q}^T \underbrace{[\mathbf{J}_{T,r} - \mathbf{J}_{T,a}]^T[\mathbf{J}_{T,r} - \mathbf{J}_{T,a}]}_{\mathbf{A}}\dot{\mathbf{q}} \,, \\ \dot{g}_T &= \mathbf{v}_{s1}^T\mathbf{t}_1 + \mathbf{v}_{s2}^T\mathbf{n}_2 = \delta^{-1}\mathbf{q}^T \underbrace{[\mathbf{J}_{T,r} - \mathbf{J}_{T,a}]^T\widetilde{\mathbf{e}}_3^T[\mathbf{J}_{T,r} - \mathbf{J}_{T,a}]}_{\mathbf{B}}\dot{\mathbf{q}} + \underbrace{r_r\mathbf{e}_3^T\mathbf{J}_{R,r}}_{\mathbf{c}}\dot{\mathbf{q}} \,. \end{aligned} \tag{7}$$

g_N is the norm of the distance, $\dot{g}_N$, $\dot{g}_T$ are the norm of the tangential and relative velocity, respectively. After the analysis of the contact kinematics the total differential of Eq. (7) will be discretized (first order Taylor approximation)

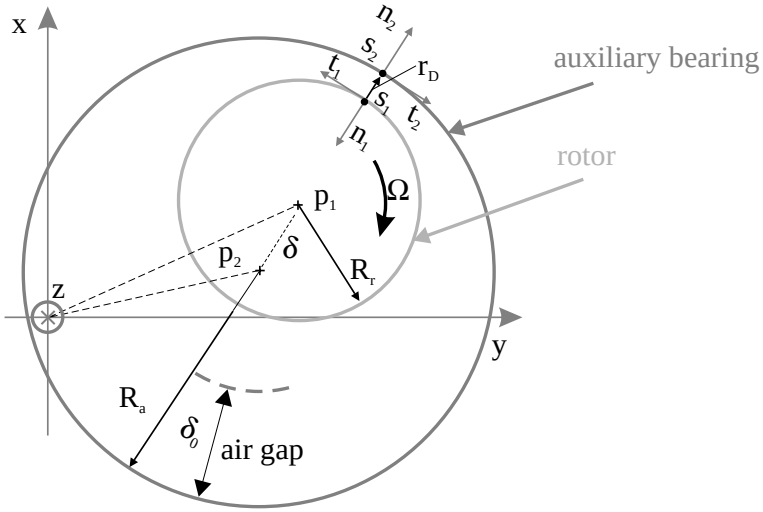

Fig. 4. Planar contacty.

as already formulated in Stiegelmeyr [13]. The following difference relations were used to obtain the previou equation:

$$
\begin{aligned}
dg_N(\mathbf{q}) &= \underbrace{\frac{\partial g_N}{\partial \mathbf{q}}}_{\mathbf{w}_N^T} d\mathbf{q} \qquad\qquad \rightarrow \quad \Delta g_N(\mathbf{q}) = \mathbf{W}_N^T \Delta\mathbf{q} + O(2)\,, \\
d\dot{g}_N(\dot{\mathbf{q}},\mathbf{q}) &= \underbrace{\frac{\partial \dot{g}_N}{\partial \dot{\mathbf{q}}}}_{\mathbf{w}_N^T} d\dot{\mathbf{q}} + \underbrace{\frac{\partial \dot{g}_N}{\partial \mathbf{q}}}_{\widehat{\mathbf{w}}_N^T} d\mathbf{q} \rightarrow \Delta\dot{g}_N(\dot{\mathbf{q}},\mathbf{q}) = \mathbf{W}_N^T \Delta\dot{\mathbf{q}} + \widehat{\mathbf{W}}_N^T \Delta\mathbf{q} + O(2)\,, \\
d\dot{g}_T(\dot{\mathbf{q}},\mathbf{q}) &= \underbrace{\frac{\partial \dot{g}_T}{\partial \dot{\mathbf{q}}}}_{\mathbf{w}_T^T} d\dot{\mathbf{q}} + \underbrace{\frac{\partial \dot{g}_T}{\partial \mathbf{q}}}_{\widehat{\mathbf{w}}_T^T} d\mathbf{q} \;\rightarrow \Delta\dot{g}_T(\dot{\mathbf{q}},\mathbf{q}) = \mathbf{W}_T^T \Delta\dot{\mathbf{q}} + \widehat{\mathbf{W}}_T^T \Delta\mathbf{q} + O(2)\,,
\end{aligned}
\tag{8}
$$

$$
\begin{aligned}
&\mathbf{W}_N = -\delta^{-1}\mathbf{A}\mathbf{q} \qquad \mathbf{W}_T = \delta^{-1}[\mathbf{B}^T\mathbf{q} + \delta\mathbf{c}^T]\,, \\
&\widehat{\mathbf{W}}_N = \delta^{-1}[\dot{g}_N\mathbf{W}_N - \mathbf{A}\dot{\mathbf{q}}] \quad \widehat{\mathbf{W}}_T = \delta^{-1}[(\dot{g}_T - \mathbf{c}\dot{\mathbf{q}})\mathbf{W}_N + \mathbf{B}\dot{\mathbf{q}}]\,.
\end{aligned}
\tag{9}
$$

With the help of:

$$
\begin{aligned}
\Delta\mathbf{q} &= \mathbf{q}(t+\Delta t) - \mathbf{q}(t) = \mathbf{q}^{l+1} - \mathbf{q}^l\,, \\
\Delta g_N &= g_N(\mathbf{q}+\Delta\mathbf{q}) - g_N(\mathbf{q}) = g_N^{l+1} - g_N^l\,, \\
\Delta\dot{g}_N &= g_N(\dot{\mathbf{q}}+\Delta\dot{\mathbf{q}},\mathbf{q}+\Delta\mathbf{q}) - g_N(\dot{\mathbf{q}},\mathbf{q}) = \dot{g}_N^{l+1} - \dot{g}_N^l\,, \\
\Delta\dot{g}_T &= g_T(\dot{\mathbf{q}}+\Delta\dot{\mathbf{q}},\mathbf{q}+\Delta\mathbf{q}) - g_T(\dot{\mathbf{q}},\mathbf{q}) = \dot{g}_T^{l+1} - \dot{g}_T^l\,.
\end{aligned}
$$

3.0.1. Unilateral constrain force

The equation of motion with unilateral contact can be written in the following compact form:

$$
\mathbf{M}\ddot{\mathbf{q}} = -\mathbf{h}(\dot{\mathbf{q}},\mathbf{q},t) + \mathbf{W}_N^T\lambda_N + \mathbf{W}_T^T\lambda_T\,. \tag{10}
$$

Here λ_N and λ_T are the normal and tangential force. Vector $\mathbf{W}_N^T$ and $\mathbf{W}_T^T$ are the contact vectors from Eq. (9) which projecting the contact forces in configuration coordinates into the generalized coordinates. The vector $\mathbf{h}$ contains all gyroscopic and active forces as well as all moments and will be defined in the sections below.

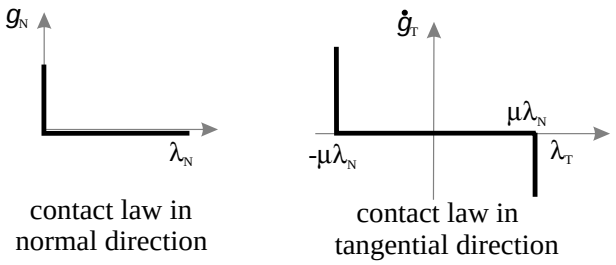

Fig. 5. Constrain force.

The discretization of the acceleration in Eq. (10) is realized through the explicit Euler formula (Eq. 11) and the velocity is discretized by the implicit rule (Eq. 12)

$$\ddot{\mathbf{q}} = \frac{\dot{\mathbf{q}}^{l+1} - \dot{\mathbf{q}}^{l}}{\Delta t} \,, \tag{11}$$

$$\begin{aligned} \dot{\mathbf{q}}^{l+1} &= \dot{\mathbf{q}}^{l} + \mathbf{M}^{-1}[\mathbf{h} + \mathbf{W}_N^T \lambda_N + \mathbf{W}_T^T \lambda_T]\Delta t \,, \\ \mathbf{q}^{l+1} &= \mathbf{q}^{l} + \dot{\mathbf{q}}^{l+1}\Delta t \,. \end{aligned} \tag{12}$$

Equations (10), (11), (12) were inserted in Eq. (8) leading to Eq. (13)

$$\begin{bmatrix} g_N \\ \dot{g}_T \end{bmatrix}^{l+1} = \begin{bmatrix} G_{NN}\Delta t & G_{NT}\Delta t \\ G_{TN} & G_{TT} \end{bmatrix} \begin{bmatrix} \Lambda_N \\ \Lambda_T \end{bmatrix} + \begin{bmatrix} \mathbf{G}_N \\ \mathbf{G}_T \end{bmatrix} \mathbf{H}\Delta t + \begin{bmatrix} r_N \\ r_T \end{bmatrix} + \begin{bmatrix} g_N \\ \dot{g}_T \end{bmatrix}^{l} \,. \tag{13}$$

The forces were multiplied bei Δt, $\Lambda_N = \lambda_N \Delta t$, $\Lambda_T = \lambda_T \Delta t$ and $\mathbf{H} = \mathbf{h}\Delta t$. More abbreviations are listed below:

$$\begin{aligned} \mathbf{G}_N = \mathbf{W}_N^T \mathbf{M}^{-1} \,;\; \mathbf{G}_T = [\mathbf{W}_T + \widehat{\mathbf{W}}_T \Delta t]^T \mathbf{M}^{-1} \,, \\ G_{NN} = \mathbf{G}_N \mathbf{W}_N \,;\; G_{NT} = \mathbf{G}_N \mathbf{W}_T \,;\; G_{TN} = \mathbf{G}_T \mathbf{W}_N \,;\; G_{TT} = \mathbf{G}_T \mathbf{W}_T \,, \\ r_N = \mathbf{W}_N^T \dot{\mathbf{q}}^l \Delta t \,;\; r_T = \widehat{\mathbf{W}}_T^T \dot{\mathbf{q}}^l \Delta t \,. \end{aligned}$$

The calculation of the momentum Λ_N, Λ_T, and accordingly the normal and tangential forces λ_N, λ_T are derived from Fig. 5 and determined as follows.

$$\begin{aligned} g_N^{l+1} \geqslant 0 \; \lambda_N \geqslant 0 \qquad & g_N^{l+1} \lambda_N = 0 \,, \\ \dot{g}_T^{l+1} = 0 \qquad & \mid \lambda_T \mid - \mu \lambda_N \leqslant 0 \,, \\ \dot{g}_T^{l+1} \neq 0 \qquad & \lambda_T + \operatorname{sign}(\dot{g}_T^{l+1})\, \mu \lambda_N = 0 \,. \end{aligned} \tag{14}$$

3.0.2. Poisson's impact law

The classical theory of impact explains that this phenomenon are related to a sudden changes in the motion state of a given mass. These impacts are dealt with on the momentum level. Because the impact is a physical process that happens on the velocity level. To do this Eq. (10) is reformulated as an equivalent mass equation

$$\mathbf{M} d\dot{\mathbf{q}} + d\mathbf{H} - \mathbf{W}_N d\Lambda_N - \mathbf{W}_T d\Lambda_T = \mathbf{0} \,. \tag{15}$$

The discretization of the Eq. (15) has been previously presented by Stiegelmeyr [13]. The author assumes that the impact time in real systems is finite and therefore the part of the momentum $d\mathbf{H}$ can not be disregarded. Using Poisson's law the impact process will be separated into a compression and an expansion phase. The compression starts at time t_A and ends at t_C. The expansion follows immediately and ends at time t_E. The Equation (15) bases on the discrete compression time $\tau_C = t_C - t_A$, so that $(d \to \Delta)$

$$\begin{aligned} \mathbf{M} \underbrace{\Delta \dot{q}}_{\mathbf{q_C} - \mathbf{q_A}} &= \underbrace{\Delta \mathbf{H}}_{\mathbf{H}_C} + \mathbf{W}_N \underbrace{\Delta \Lambda_N}_{\Lambda_{NC}} + \mathbf{W}_T \underbrace{\Delta \Lambda_T}_{\Lambda_{TC}} \,, \\ \mathbf{q}_C - \mathbf{q}_A &= \mathbf{q}_C \tau_C \,. \end{aligned} \tag{16}$$

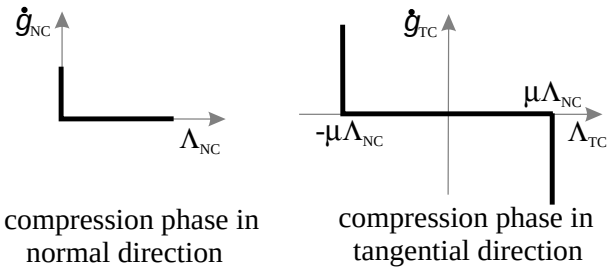

Fig. 6. Contact law for the compression phase.

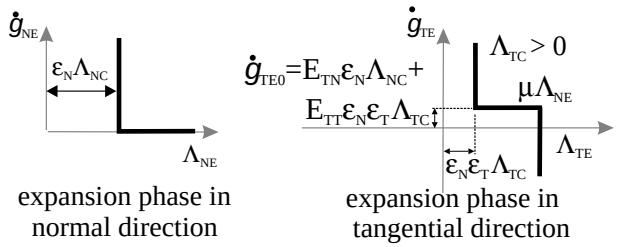

Fig. 7. Contact law for the expanssion phase.

The relative velocity at the end of the compression phase $\dot{\mathbf{g}}_{NC}$, $\dot{\mathbf{g}}_{TC}$, can be calculated analogously to Eq. (13)

$$\begin{bmatrix}\dot{g}_{NC}\\ \dot{g}_{TC}\end{bmatrix} = \begin{bmatrix}C_{NN}\ C_{NT}\\ C_{TN}\ G_{TT}\end{bmatrix}\begin{bmatrix}\Lambda_{NC}\\ \Lambda_{TC}\end{bmatrix} + \begin{bmatrix}\mathbf{C}_N\\ \mathbf{C}_T\end{bmatrix}\mathbf{H}_C + \begin{bmatrix}r_{NC}\\ r_{TC}\end{bmatrix} + \begin{bmatrix}\dot{g}_A\\ \dot{g}_A\end{bmatrix}\ . \tag{17}$$

With the following shortcuts:

$$\mathbf{C}_N = [\mathbf{W}_N + \widehat{\mathbf{W}_N}\tau_C]^T\mathbf{M}^{-1}\ ;\ \mathbf{C}_T = [\mathbf{W}_T + \widehat{\mathbf{W}}_T\tau_C]^T\mathbf{M}^{-1}\ ;$$
$$C_{NN} = \mathbf{C}_N\mathbf{W}_N\ ;\ C_{NT} = \mathbf{C}_N\mathbf{W}_T\ ;\ C_{TN} = \mathbf{C}_T\mathbf{W}_N\ ;\ C_{TT} = \mathbf{G}_T\mathbf{W}_T\ ;$$
$$r_{NC} = \widehat{\mathbf{W}}_N^T\dot{\mathbf{q}}_A\tau_C\ ;\ r_{TC} = \widehat{\mathbf{W}}_T^T\dot{\mathbf{q}}_A\tau_C\ .$$

Figure 6 shows the contact law for the compression phase in normal and tangential contact direction, which are defined by

$$\begin{aligned}&\dot{g}_{NC} \geqslant 0\ \ \Lambda_{NC} \geqslant 0\ , && g_{NC}\Lambda_{NC} = 0\ ,\\ &\dot{g}_{TC} = 0\ , && \mid \Lambda_{TC} \mid -\mu\Lambda_{NC} \leqslant 0\ ,\\ &\dot{g}_{TC} \neq 0\ , && \Lambda_{TC} + \operatorname{sign}(\dot{g}_{TC})\ \mu\Lambda_{NC} = 0\ .\end{aligned} \tag{18}$$

The relative velocity at the end of the expansion phase $\dot{g}_{NE}$, $\dot{g}_{TE}$ possesses the same structure as in the compression phase in Eq. (17). Swapping of the indices in Eq. (17) ($C \to E, A \to C, \tau_C \to \tau_E$) with the discrete expansion time $\tau_E = t_E - t_C$, one gets

$$\begin{bmatrix}\dot{g}_{NE}\\ \dot{g}_{TE}\end{bmatrix} = \begin{bmatrix}E_{NN}\ E_{NT}\\ E_{TN}\ E_{TT}\end{bmatrix}\begin{bmatrix}\Lambda_{NE}\\ \Lambda_{TE}\end{bmatrix} + \begin{bmatrix}\mathbf{E}_N\\ \mathbf{E}_T\end{bmatrix}\mathbf{H}_E + \begin{bmatrix}r_{NE}\\ r_{TE}\end{bmatrix} + \begin{bmatrix}\dot{g}_{NC}\\ \dot{g}_{TC}\end{bmatrix}\ . \tag{19}$$

During the expansion phase Poisson's impact law was used in normal direction with ($\Lambda_{NE} = \varepsilon_N\Lambda_{NC}$). Here ε_N is the dissipation coefficient. The expansion law in tangential direction has been adopted from Beitelschmit [1].

3.0.3. Active rotor-auxiliary bearing to be controlled

The complete equation of motions is written as HMBS (rigid body and elastic subsystem), whereas coupling between rotor and active auxiliary bearing exists only during the appearance of contact forces. The evaluation of the mechanical impact dynamics is based on the rigid-body contact approach, which is described as constraints between

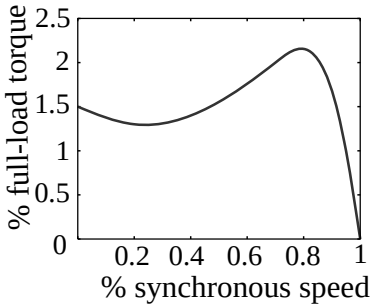

Fig. 8. Speed torque curve.

contact forces and relative kinematics. This method allows the calculation of the normal and tangential momentum by means of an implicit and explicit discretization (time-stepping algorithm).

By considering

$$\underbrace{\begin{bmatrix}\mathbf{M}_r & \mathbf{0}\\ \mathbf{0} & \mathbf{M}_a\end{bmatrix}}_{\mathbf{M}}\underbrace{\begin{bmatrix}\ddot{\mathbf{q}}_r\\ \ddot{\mathbf{q}}_a\end{bmatrix}}_{\ddot{\mathbf{q}}}+\underbrace{\begin{bmatrix}\mathbf{D}_r+\mathbf{G}_r(\Omega) & \mathbf{0}\\ \mathbf{0} & \mathbf{D}_a\end{bmatrix}}_{\mathbf{D}}\underbrace{\begin{bmatrix}\dot{\mathbf{q}}_r\\ \dot{\mathbf{q}}_a\end{bmatrix}}_{\dot{\mathbf{q}}}+\underbrace{\begin{bmatrix}\mathbf{S}_r+\mathbf{N}_r(\Omega,\dot{\Omega}) & \mathbf{0}\\ \mathbf{0} & \mathbf{0}\end{bmatrix}}_{\mathbf{S}}\underbrace{\begin{bmatrix}\mathbf{q}_r\\ \mathbf{q}_a\end{bmatrix}}_{\mathbf{q}}$$

and

$$\mathbf{h}(\dot{\mathbf{q}},\mathbf{q},\mathbf{i})=\underbrace{-\mathbf{D}\dot{\mathbf{q}}-\mathbf{S}\mathbf{q}+\mathbf{J}_{T,r}^T\,\mathbf{f}_{unb}+\mathbf{J}_{T,r}^T\,\mathbf{f}_{mag}|_{z=z_m}+\mathbf{J}_{R,r}^T\,\mathbf{l}_{mot}|_{z=z_d}}_{\mathbf{h}_q}+\mathbf{J}_{T,a}^T\,\mathbf{u}_a\ ,$$

$$\mathbf{W}\lambda=\begin{bmatrix}\mathbf{W}_N\ \mathbf{W}_T\end{bmatrix}\begin{bmatrix}\lambda_N\\ \lambda_T\end{bmatrix}\ ,$$

the equation of motion can be described in compact form as

$$\begin{aligned}\ddot{\mathbf{q}}&=\underbrace{\mathbf{M}^{-1}\left(\mathbf{h}_q+\mathbf{W}\lambda\right)}_{\mathbf{f}}+\underbrace{\mathbf{M}^{-1}\mathbf{J}_{F,a}^T}_{\mathbf{B}}\,\mathbf{u}_a\ ,\\ &=\mathbf{f}(\dot{\mathbf{q}},\mathbf{q},t)+\mathbf{B}\,\mathbf{u}_a\end{aligned}\tag{20}$$

where $\mathbf{M}$ is the mass matrix, $\mathbf{D}$ stands for both the damping and skew gyroscopic matrix and $\mathbf{S}$ represents is the stiffness and skew circulatory matrix. The vectors $\mathbf{f}_{unb}$, $\mathbf{f}_{mag}$ and $\mathbf{l}_{mot}$ are the unbalanced force, the magnet bearing force and the torque of the drive motor. The characteristic curve of the torque is shown in Fig. 8.

The vector $\mathbf{h}$ contains all gyroscopic effects, as well as all active forces and moments, and is composed by $\mathbf{h}_q$ and the control force vector $\mathbf{u}_a$. $\mathbf{J}_{T,r}$, $\mathbf{J}_{R,r}$ and $\mathbf{J}_{T,f}$ which have been described in Eq. (5) are the Jacobi matrices at the magnetic bearing ($z=z_{mag}$) and at the torque ($z=z_{mot}$) as can be seen in Fig. 1. The constrain matrix is $\mathbf{W}$ and the vector of the contact force is λ.

4. Control concept

The control concept was designed such that the movement of the active auxiliary bearing will be synchronized to the rotor orbit just before the occurrence of a contact. After contact the control has to assure a smooth transition to the permanent contact condition, keeping the contact forces as small as possible and avoiding multi-contacts.

$$\mathbf{u}_a=\underset{(\ddot{\mathbf{q}},\dot{\mathbf{q}},\mathbf{q})}{\arg\min}\begin{cases}g_N\\ \dot{g}_N\end{cases}\tag{21}$$

where $arg\ min\ \mathbf{g}(.)=$ value of $(.)$ that minimizes $\mathbf{g}(.)$.

The $\dot{g}_T$ will not be taken into consideration in Eq. (21) because a non-sliding contact would demand a very high backward whirl (Ω_{bw}) compared with the speed of rotation (Ω), because the size of the air gap (δ_0), relative to the outer diameter of the rotor, R_r, is small:

$$\dot{g}_T = 0 \quad \rightarrow \quad \Omega_{bw} = -\left(\frac{R_r}{\delta_0}\right)\Omega \; . \tag{22}$$

4.0.4. Sliding control

The main idea of sliding control as explained in Khalil [8], Slotine and Le [11], Friedland [5], is the transformation of tracking error into a problem of stabilizing a time dependent surface, which will be presented in this section.

The sliding control strategy is designed in such a way that the auxiliary bearing tracks the given rotor trajectory to assure the reduction of the impact when the first contact occurs. The mathematical description of the system in the case of no contact (Eq. 20 with $\lambda = \mathbf{0}$) is

$$\ddot{\mathbf{q}} = \mathbf{M}^{-1}\mathbf{h}_q + \mathbf{M}^{-1}\mathbf{J}_{T,a}^T\mathbf{u}_a \; . \tag{23}$$

The x-, y-acceleration of the rotor and auxiliary bearing is expressed by using the vector q of the generalized coordinates and the Jacobian matrix of translation as

$$\begin{aligned} \ddot{\mathbf{r}}_r &= \mathbf{J}_{T,r}\mathbf{M}^{-1}\mathbf{h}_q \; , \\ \ddot{\mathbf{r}}_a &= \mathbf{J}_{T,a}\mathbf{M}^{-1}\mathbf{h}_q + \mathbf{J}_{T,a}\mathbf{M}^{-1}\mathbf{J}_{T,a}^T\mathbf{u}_a \; , \end{aligned} \tag{24}$$

so that $\mathbf{J}_{T,r}\mathbf{M}^{-1}\mathbf{J}_{T,a}^T = \mathbf{0}$.

The vectors of the contact points $s_1,\ s_2$ in Fig. 4 can be formulated as

$$\begin{aligned} &\mathbf{r}_{s_1} = \mathbf{r}_r - \mathbf{n}_1 R_r \quad ; \quad \mathbf{r}_{s_2} = \mathbf{r}_a + \mathbf{n}_2 R_a \; ; \\ &\widetilde{\mathbf{r}} = \mathbf{r}_{s_1} - \mathbf{r}_{s_2} \; . \end{aligned} \tag{25}$$

The vector $\widetilde{\mathbf{r}}$ defines the tracking error between the vector $\mathbf{r}_r$ and the time variant vector $\mathbf{r}_a$. Introducing

$$\mathbf{R} = [\,\widetilde{\mathbf{r}}^{\,T} \quad \dot{\widetilde{\mathbf{r}}}^{\,T}\,]^{\,T} \tag{26}$$

then the time variant surface **s** is established by

$$\mathbf{s}(\mathbf{R};t) = \dot{\widetilde{\mathbf{r}}} + \mathrm{diag}(\psi)\,\widetilde{\mathbf{r}} \; . \tag{27}$$

where $\mathrm{diag}(\psi)$ is a diagonal positive-definite matrix. If the condition $\mathbf{s} \rightarrow \mathbf{0}$ and $\dot{\mathbf{s}} \rightarrow \mathbf{0}$ are met then the stabilization of the surfaces **s** can be assured. The calculation of **s** can be done after the reorganization of Eq. (23) and the derivation of Eq. (26). The vector function $\mathbf{h}_q$ in Eq. (23) is not exactly know because the stimulation of the magnetic bearing, but it is estimated by $\widehat{\mathbf{h}}_q$. The best approximation to a continuous control law is

$$\widehat{\mathbf{u}}_a = \mathbf{J}_{T,a}\mathbf{M}\mathbf{J}_{T,a}^T[\ddot{\mathbf{r}}_r + \mathrm{diag}(\psi)\dot{\widetilde{\mathbf{r}}} - \mathbf{J}_{T,a}\mathbf{M}^{-1}\widehat{\mathbf{h}}_q - \ddot{\mathbf{n}}_1\,\delta_0] \; . \tag{28}$$

In order to remove the discontinuity along **s** (chattering effect) caused by the controller, a boundary layer was defined with positive vector ϕ

$$\mathbf{B}(t) = \{\mathbf{R},\ \mathbf{s}(\mathbf{R};t) \leqslant \phi\} \; . \tag{29}$$

Each component in the boundary layer thickness (ϕ_i) will be attractive if the controller fulfills the following criteria:

$$\left.\begin{array}{l} s_i \geqslant \ \phi_i \rightarrow \frac{d}{dt}(s_i - \phi_i) \leqslant -n_i \\ s_i \leqslant -\phi_i \rightarrow \frac{d}{dt}(s_i - \phi_i) \geqslant \ n_i \end{array} \quad i = 1,2 \right\} \ |s_i| \geqslant \phi_i \Rightarrow \frac{d}{dt}s_i \leqslant \dot{\phi}_i - \eta_i \leqslant 0 \tag{30}$$

Where η_i is a strictly positive constant. On the other hand, the gain vectors are defined as

$$\begin{aligned}\mathbf{k} &= \underbrace{|\mathbf{J}_{T,a}\mathbf{M}(\mathbf{h}_q - \widehat{\mathbf{h}}_q)|}_{\bar{\mathbf{h}}} + \eta = \bar{\mathbf{h}} + \eta \,, \\ \bar{\mathbf{k}} &= \mathbf{k} - \dot{\phi} \,.\end{aligned} \tag{31}$$

Next, the sliding control will be introduced

$$\mathbf{u}_a = \widehat{\mathbf{u}}_a - \mathrm{diag}(\bar{\mathbf{k}})\mathrm{sat}[\mathrm{diag}(\phi)^{-1}\mathbf{s}] \,. \tag{32}$$

The controller guarantees that the distance to the boundary layer always decreases in case of $|\mathbf{s}| > \phi$ and

$$\begin{aligned} V(\mathbf{s}) &= \frac{1}{2}\mathbf{s}^T\mathbf{s} \,, \\ \frac{d}{dt}V(\mathbf{s}) &= \mathbf{s}^T\left[\mathbf{J}_{T,a}\mathbf{M}(\mathbf{h}_q - \widehat{\mathbf{h}}_q) - \mathrm{diag}(\bar{\mathbf{k}})\mathrm{sat}[\mathrm{diag}(\phi)^{-1}\mathbf{s}]\right] \\ &\leqslant \mathbf{s}^T[\bar{\mathbf{h}} - \mathrm{diag}(\bar{\mathbf{h}})\mathrm{sign}(\mathbf{s})] + \mathbf{s}^T[\mathrm{diag}(\dot{\phi} - \eta)\mathrm{sign}(\mathbf{s})] \\ &\leqslant \mathbf{s}^T\mathrm{diag}(\dot{\phi} - \eta)\mathrm{sign}(\mathbf{s}) \leqslant \mathbf{0} \,. \end{aligned} \tag{33}$$

The system trajectories inside the boundary layer $|\mathbf{s}| \leqslant \phi$ from Eq. (27)

$$\dot{\mathbf{s}} + \mathrm{diag}(\bar{\mathbf{k}})\mathrm{diag}(\phi)^{-1}\mathbf{s} = \bar{\mathbf{h}} \,. \tag{34}$$

The boundary layer thickness ϕ is formulated as a first-order filter with the help of the gain vector ψ

$$\begin{aligned}\bar{\mathbf{k}} &= \mathrm{diag}(\psi)\phi \,, \\ \mathbf{k} &= \dot{\phi} + \mathrm{diag}(\psi)\phi \,.\end{aligned} \tag{35}$$

Equation (35) defines the time-history of the boundary layer thickness ϕ.

4.1. Feedback linearization and cross coupled feedback

The force-field curve of the actuator, obtained by the variation of the magnetic force due to control current and the displacement of the shaft relative to the actuator casing, will be mapped to the required control force by use of the feedback-linearization method. The basic principles are stated in Khalil [8], Slotine and Le [11].

The so linearized actuator is being used for two applications. First, the actuator is used in connection with the auxiliary bearing to stabilize the system when it comes to rubbing and to minimize contact forces as previously explained. Second, it is used to simulate the behavior of a passive rotor-auxiliary bearing system.

The cross coupled feedback is activated after the occurrence of the first small impact. The control law is:

$$\mathbf{u}_a = -k\,\widetilde{\mathbf{e}}_3\mathbf{J}_{T,a}\dot{\mathbf{q}} \,. \tag{36}$$

With $\widetilde{\mathbf{e}}_3$, $\mathbf{J}_{T,f}$ and $\dot{\mathbf{q}}$ according to the Eq. (6), Eq. (5), Eq. (4), respectively and the gain control k.

If the condition of permanent sliding contact is assumed ($\dot{g}_T > 0$), the Coulomb friction model can be used ($\lambda_N = -\mu\lambda_T$). Next, the control law (Eq. 36) can be inserted in Eq. (20) and can then be reformulated as a close-loop equation of motion

$$\begin{aligned}\ddot{\mathbf{q}} &= -\mathbf{M}^{-1}\underbrace{[\mathbf{D} + k\,\mathbf{J}_{T,a}^T\widetilde{\mathbf{e}}_3\mathbf{J}_{T,a}]}_{\mathbf{D}^*(k)}\dot{\mathbf{q}} - \mathbf{M}^{-1}\underbrace{[\mathbf{S} + \delta^{-1}(\mathbf{A} + \mu\mathbf{B}^T)\lambda_N]}_{\mathbf{S}^*(\lambda_N)}\mathbf{q} + ... \\ &\quad \underbrace{\mathbf{M}^{-1}[\mathbf{J}_{T,r}^T\mathbf{f}_{unb} + \mathbf{J}_{T,r}^T\mathbf{f}_{mag}]}_{\mathbf{h}^*(\dot{\Omega},\Omega)} + \underbrace{\mathbf{M}^{-1}\mathbf{J}_{R,r}^T[\mathbf{l}_{mot} - \mu R_r\lambda_N\mathbf{e}_3]}_{\mathbf{l}^*(\Omega,\lambda_N)} \,, \\ &= -\mathbf{M}^{-1}\mathbf{D}^*(k)\dot{\mathbf{q}} - \mathbf{M}^{-1}\mathbf{S}^*(\lambda_N)\mathbf{q} + \mathbf{h}^*(\dot{\Omega},\Omega) + \mathbf{l}^*(\Omega,\lambda_N) \,,\end{aligned} \tag{37}$$

with

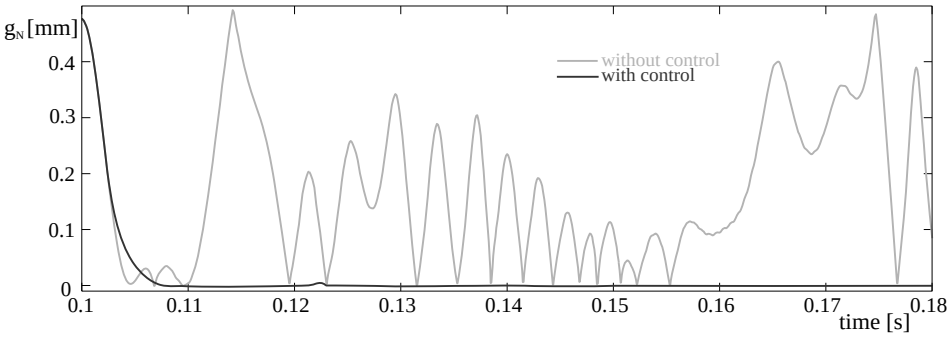

Fig. 9. Relative displacement.

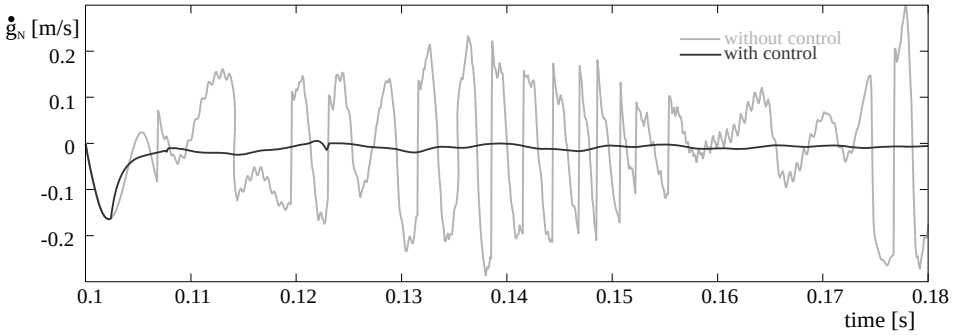

Fig. 10. Relative normal velocity.

$$k = k_0(\dot{g}_N) + k_1(\lambda_N) \; .$$

The factor k has to be determined to provide a smooth transition from the first contact to the permanent contact condition. First, in order to avoid multi impacts, the gain control k_0 will guarantee the stabilization of the normal relative velocity (Eq. 7). Second, the gain control k_1 assures the steady state of the contact force λ_N and the indirect stabilization of the rotatory speed of the rotor, because the bending and torsion vibration are coupled (Eq. 37).

Other stabilization contact force concepts can be found in Ulbrich et al. [16], Jiang and Ulbrich [7].

5. Numerical results

The rotor-active auxiliary bearing used in the following simulation is shown in Fig. 1. First the rotor is on a steady state orbit with a constant rotatory frequency of 50 Hertz. Then after 100 ms the rotor has passed through five cycles, the magnet bearing is activated and produces a rotor amplitude larger than the air gap (0.5 mm). In order to minimize the impulse (Λ) or rather the contact force (λ) the controller is activated 4 ms before the first impacts occurs.

Figures 9–13 show the performance of the previously discussed sliding and cross coupled feedback controller. For better illustration, the results are confined to a time frame from 100 ms to 180 ms.

The first noticeable results is the reduction of the relative distance between the rotor and the auxiliary bearing g_N (Fig. 9) as well as the reduction of the relative normal velocity $\dot{g}_N$ (Fig. 10) when the controller is activated.

The same effect holds true for the impulse Λ_N in normal direction. Figure 11 displays that the rotor is subjected to multi-impacts if it will not be controlled, which leads to high normal und tangential impulses.

In summary one can say that the benefits of the controller (Fig. 12) is the strong reduction of the first contact force by means of the Sliding control, the stabilization of the contact kinematics with the help of the cross coupled feedback, guiding the rotor to a stable state.

It can be seen in the Fig. 13 (left) that in case of a passive rotor-auxiliary bearing (rotor rubbing without control), the contact force will guide the rotor to an unstable state because of a heavy coupling between transversal- and torsional

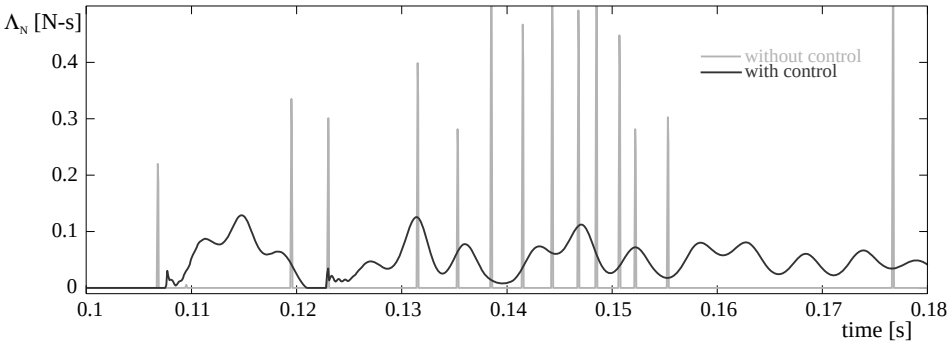

Fig. 11. Normal impulse.

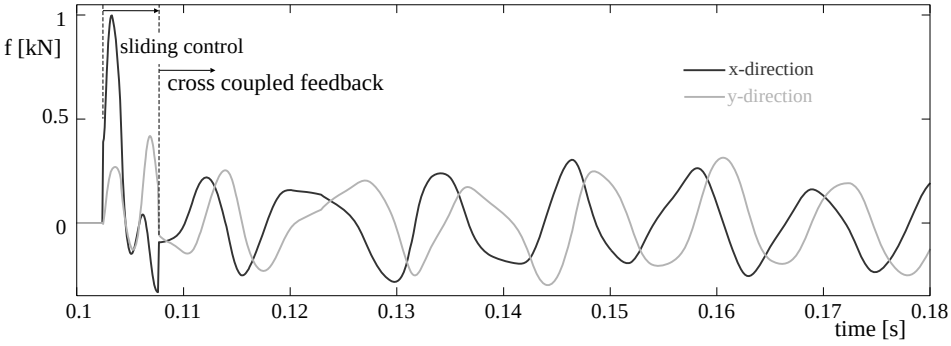

Fig. 12. Control force.

vibration and the limited drive torque. But in case of control, the angular speed Ω has also been stabilized which can be seen by the disappearance of the torsional vibration. This has been achieved by means of the piecewise constant gain control k (Eq. 36), which is composed by stabilization of the contact kinematics ($k = k_0$) and stabilization of the rotatory speed ($k = k_0 + k_1$).

In Fig. 13 (right) the orbit of the rotor for the controlled (dark line) and not controlled (light line) case is shown, between x- and y-axis in a time frame from 0.35 s to 1 s. The chaotic behavior is clearly visible when the rotor is not influenced by the controller. But with the control of the rotors a stationary, stable orbit is obtained.

6. Active rotor-auxiliary test rig

For verification of the theoretical results experiments have to be carried out. These experiments are already in progress. At the TU Munich an experimental set-up has been constructed in order to verify the theoretical work and the computer simulation, which have been presented above. The test rig can been seen in Fig. 14. Results will be published soon.

7. Conclusions and outlook

A model for a stator-rotor system has been formulated and a control concept has been developed to minimize contact forces and to bring the system into a stable state in order to prevent possible damage to men and machine.

The activated rotor-auxiliary bearing system has been modeled by the hybrid multibody system method (HMBS), which allowed to include electro-magnetic actuators in the model with its force-field and the speed-torque characteristic of the drive system.

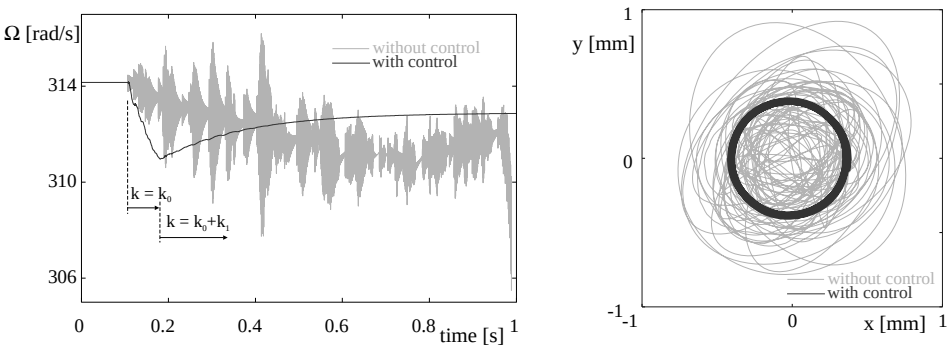

Fig. 13. Rotatory speed (left), rotor orbit (right).

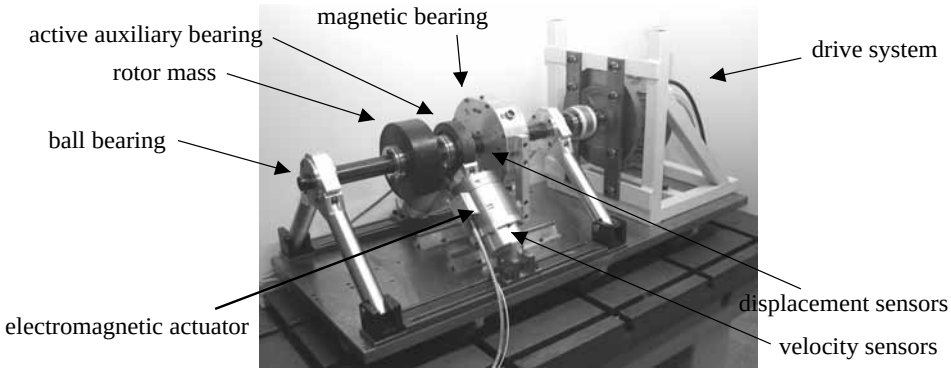

Fig. 14. Test rig at TU Munich.

The impact dynamics have been represented by a rigid body approach with the fundamental property, that for a contact the quantity of the relative kinematics is zero when the corresponding constrain forces is not zero, or vice versa.

The concept for the controller was based on the sliding control method and cross coupled feedback. It has been modified to accommodate the properties of the system in order to realize a rotor motion from the free state to permanent contact with the auxiliary bearing.

As the numerical simulations, conducted with a time stepping algorithm, have shown, it is possible not only to reduce impulses and contact forces between the rotor and the auxiliary bearing but also to bring the rotor to a stable orbit if it is perturbed by the activation of the magnetic bearing. If no interventions are made, unpredictable chaotic behavior is the unwanted result.

As mentioned above the experimental set-up has been assembled and is ready for first tests. The theoretical model as presented here and the corresponding control concept is then implemented on the test rig to show the feasibility and its practicability for such an application.

Acknowledgements

The project has been supported by the German Research Foundation (DFG). The first author is very grateful for the financial support by “Deutscher Akademischer Austausch Dienst” (DAAD) which made the research work of this paper possible.

References

[1] M. Beitelschmidt, *Reibstöße in Mehrkörpersystemen* **11**(275) (1999).

[2] H. Bremer, *Dynamik und Regelung mechanischer Systeme*, Teubner Studienbücher, Mechanik, 1988.
[3] H. Bremer and F. Pfeiffer, *Elastische Mehrkörpersysteme*, Teubner Studienbücher, Mechanik, 1992.
[4] B. Brogliato, *Nonsmooth Mechanics: Models, Dynamics and Control*, Springer, 1999.
[5] B. Friedland, *Advanced Control System Design*, Prentice Hall Publishing, 1996.
[6] C. Glocker, *Dynamik von Starrkörpersystemen mit Reibung und Stößen* **18**(82) (1995).
[7] J. Jiang and H. Ulbrich, Improvement of Rotor Performance under Rubbing Conditions Throught Active Auxiliary Bearing, *Proceedings of the 2nd International Symposium on Stability Control of Rotating Machinery*, Gdansk, Poland, 160–167.
[8] H. Khalil, *Nonlinear System*, Prentice Hall Publishing, 2002.
[9] C. Oberbeck, *Entwicklung und mechatronische Optimierung eines elektromagnestische Aktors* **8**(984) (2003).
[10] F. Pfeiffer and C. Glocker, *Multibody Dynamics With Unilateral Contacts*, Jhon Wiley & Sons, Inc., 1996.
[11] J. Slotine and W. Li, *NApplied Nonlinear Control*, Prentice Hall Publishing, 1991.
[12] A. Stiegelmeyr and F. Pfeifferh, A Time Stepping Algorithm for Mechanical System With Unilateral Contact, *Proceeding of the Design Engineering Technical Conferences, ASME*, Las Vegas, Nevada, **VIB-8348** (1999), 1–9.
[13] A. Stiegelmeyr, *Zur numerische Berechnung strukturvarianter Mehrlöpersysteme* **18**(271) (2001).
[14] A. Tornambè, Modeling and Control of Impact in Mechanical Systems: Theory and Experimental Results, *IEEE Transaction on Automatic Control* **44**(2) 294–230.
[15] H. Ulbrich, *Dynamik und Regelung von Rotorsystemen* **11**(86) (1986).
[16] H. Ulbrich, A. Chavez and R. Dhima, Minimization of Contact Forces in Case of Rotor Rubbing Using an Actively Controlled Auxiliary Bearing, *Proceedings of* 10^{th} *International Symposium on Transport Phenomena and Dynamics of Rotating Machinery*, Honolulu, Hawaii **ID 042** (2004), 1–10.
[17] A. Yigit and A. Christorouf, Coupled Torsional and Bending Vibration of Actively Controlled Drillstring, *Journal of Sound and Vibration* **234**(1), 67–83.